



Stress–strain behavior of mitral valve leaflets in the beating ovine heart

Gaurav Krishnamurthy^{a,b}, Akinobu Itoh^a, Wolfgang Bothe^a, Julia C. Swanson^a, Ellen Kuhl^b, Matts Karlsson^c, D. Craig Miller^a, Neil B. Ingels Jr.^{a,d,*}

^a Department of Cardiothoracic Surgery, Stanford University School of Medicine, Stanford, CA, USA

^b Department of Mechanical Engineering, Stanford University, Stanford, CA, USA

^c Department of Management and Engineering, Linköping University, Linköping, Sweden

^d Laboratory of Cardiovascular Physiology and Biophysics, Research Institute of the Palo Alto Medical Foundation, Palo Alto, CA, USA

ARTICLE INFO

Article history:

Accepted 10 May 2009

Keywords:

Mitral valve
Finite element analysis
Material properties
Anisotropy
Elastic modulus

ABSTRACT

Excised anterior mitral leaflets exhibit anisotropic, non-linear material behavior with pre-translational stiffness ranging from 0.06 to 0.09 N/mm² and post-translational stiffness from 2 to 9 N/mm². We used inverse finite element (FE) analysis to test, for the first time, whether the anterior mitral leaflet (AML), *in vivo*, exhibits similar non-linear behavior during isovolumic relaxation (IVR). Miniature radiopaque markers were sewn to the mitral annulus, AML, and papillary muscles in 8 sheep. Four-dimensional marker coordinates were obtained using biplane videofluoroscopic imaging during three consecutive cardiac cycles. A FE model of the AML was developed using marker coordinates at the end of isovolumic relaxation (when pressure difference across the valve is approximately zero), as the reference state. AML displacements were simulated during IVR using measured left ventricular and atrial pressures. AML elastic moduli in the radial and circumferential directions were obtained for each heartbeat by inverse FEA, minimizing the difference between simulated and measured displacements. Stress–strain curves for each beat were obtained from the FE model at incrementally increasing transmural pressure intervals during IVR. Linear regression of 24 individual stress–strain curves (8 hearts, 3 beats each) yielded a mean (\pm SD) linear correlation coefficient (r^2) of 0.994 ± 0.003 for the circumferential direction and 0.995 ± 0.003 for the radial direction. Thus, unlike isolated leaflets, the AML, *in vivo*, operates linearly over a physiologic range of pressures in the closed mitral valve.

© 2009 Elsevier Ltd. All rights reserved.

1. Introduction

The mitral valve has a dual role during left ventricular (LV) systole in the beating heart. The mitral leaflets, the key components of the valve, must maintain appropriate relative positions and geometry during systole to (1) seal tightly to prevent regurgitant backflow from the LV into the left atrium (LA) and (2) provide an appropriately shaped portion of the LV outflow tract. The material properties of the leaflets are of critical importance to both of these tasks, as the varying demands on the heart are met with a wide range of LV pressures and volumes.

The material properties of excised mitral leaflets have been well-characterized (Kunzelman and Cochran, 1992; May-Newman and Yin, 1995; Chen et al., 2004a,b; He et al., 2003; Sacks et al., 2002, 2006; He et al., 2005). In uniaxial studies of excised leaflets, Kunzelman and Cochran (1992) measured highly non-linear

stress–strain behavior with distinct pre- and post-translational regions. In biaxial studies of excised anterior leaflets, May-Newman and Yin (1995) found anisotropic, non-linear material properties with pre-translational stiffness values ranging from 0.06 to 0.09 N/mm² and post-translational stiffness values from 2 to 9 N/mm². Recent mitral valve models (Kunzelman et al., 2007; Prot et al., 2007; Votta et al., 2008) have incorporated these leaflet data into hyperelastic finite element analyses (FEA). Sacks et al. (2002) used a left heart simulator and graphite markers to study the *in vitro* surface strains in the porcine anterior mitral valve leaflets and showed a non-linear relationship between transmural pressures and leaflet areal strains. The first attempt at quantifying *in vivo* leaflet strains by Sacks et al. (2006) using a sonomicrometry transducer array showed the same non-linear relationship between pressure and leaflet strains in ovine anterior mitral valve leaflets. Sacks and Enomoto (2006) computed only *in vivo* leaflet strains and did not determine the *in vivo* leaflet elastic moduli or show the relationship between leaflet stresses and leaflet strains for the beating heart.

Recently, we used inverse FEA to obtain the anisotropic elastic moduli of anterior mitral valve leaflets during isovolumic relaxation (IVR) in the beating ovine heart (Krishnamurthy et al.,

* Corresponding author at: Laboratory of Cardiovascular Physiology and Biophysics, Research Institute of the Palo Alto Medical Foundation, Palo Alto, CA, USA. Tel.: +1 650 853 4834; fax: +1 650 324 2665.

E-mail address: ingels@stanford.edu (N.B. Ingels Jr.).

2008). As a first approximation, we assumed a linear relationship between stress and strain during IVR. The present study was undertaken to test the validity of this assumption.

2. Methods

All animals received humane care in compliance with the “Principles of Laboratory Animal Care” formulated by the National Society for Medical Research and also in compliance with the “Guide for the Care and Use of Laboratory Animals” prepared by the National Academy of Sciences and published by the National Institutes of Health (US Department of Health and Human Services, NIH Publication 85-23, Revised 1985). This study was approved by the Stanford Medical Center Laboratory Research Animal Preview Committee, which is accredited by the Association for Assessment and Accreditation of Laboratory Animal Care International, and conducted according to Stanford University policy.

2.1. Surgical preparation

Eight adult, Dorsett-hybrid, male sheep (56±8 kg) were premedicated with ketamine (25 mg/kg intramuscularly) for venous and arterial catheter placement and monitoring. Anesthesia was induced and maintained with inhalational isoflurane (1–2.5%) and supplemental oxygen. Through a left thoracotomy, 13 miniature tantalum radiopaque markers were implanted in the left-ventricle (LV) subepicardial wall silhouetting the LV chamber (Fig. 1A). Via a left atriotomy with cardiopulmonary bypass and antegrade cardioplegic arrest, a total of 35 radiopaque tantalum markers were sewn to the following sites: 16 on the atrial aspect of the anterior mitral leaflet (AML) (7 on the AML edge (#1–7; Fig. 1B); 9 on the leaflet belly (#8–16; Fig. 1B)), 16 around the mitral annulus (Fig. 1A), 1 on the central edge of the middle scallop of the posterior mitral leaflet (PML; Fig. 1A), and 2 on the anterolateral and posteromedial papillary muscle tips (APM, PPM; Fig. 1A). A micromanometer pressure transducer (PA4.5-X6, Konigsberg instruments, Inc., Pasadena, CA, USA) was placed in the LV chamber through the left atrium and exteriorized.

2.2. Data acquisition

Immediately after the operation, the animals were transferred to the catheterization laboratory and studied in the right lateral decubitus position with the chest open. Two micromanometer-tipped pressure transducers (model MPC-500; Millar Instruments, Houston, TX, USA) were calibrated and inserted into the LV and ascending aorta via a carotid artery catheter, respectively. A Konigsberg pressure transducer was calibrated against the two Millar pressure transducers while all transducers were in the LV, then pulled back into the LA to record left atrial pressure (LAP). Simultaneous biplane videofluoroscopic images (60 Hz, Philips Medical Systems, Pleasanton, CA, USA), ECG, LV pressure (LVP), aortic pressure and LAP were recorded during a hemodynamically stable interval with the heart in normal sinus rhythm and ventilation transiently arrested at end-

expiration. At the completion of each study biplane images of a 3D helical phantom of known dimensions spanning the heart space were recorded. The 2D coordinates of each marker in each projection image were digitized frame-by-frame, using semi-automated image processing and digitization software developed in our laboratory (Niczyporuk and Miller, 1991). Data from the two views were merged using the 3D helical phantom image data and software, described previously, and used to yield the 3D marker coordinates (Daughters et al., 1989). The accuracy of the 3D reconstructions from biplane videograms of length measurements was previously shown to be 0.1±0.3 mm (Daughters et al., 1989).

2.3. Hemodynamics and cardiac cycle timing

Three consecutive beats in sinus rhythm were selected for analysis from each heart. For each beat, end-systole (ES) was defined as the frame containing the minimum second derivative of LVP with respect to time during IVR. Negative dP/dt_{max} was computed as the maximum time derivative of LVP during IVR. The onset of isovolumic relaxation (IVR₁; Fig. 2) was defined at ES and the end of isovolumic relaxation (IVR₂; Fig. 2) as the frame immediately before mitral valve opening.

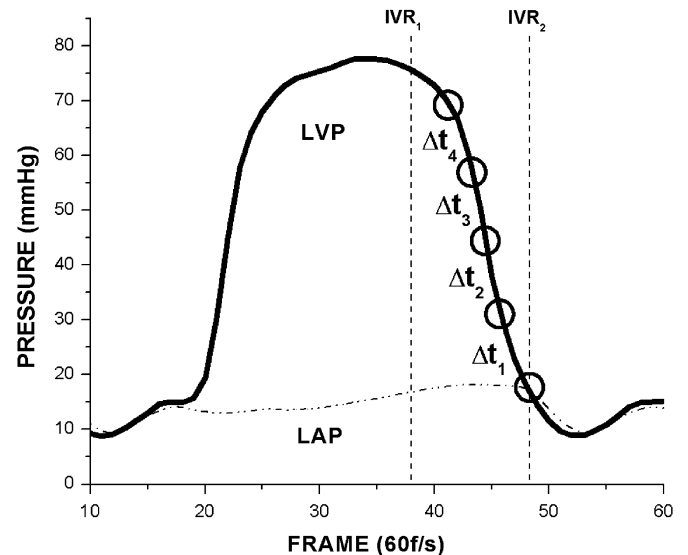


Fig. 2. LVP, LAP and time-steps. Left ventricular pressure (LVP) and left atrial pressure (LAP) shown for one cardiac cycle. Isovolumic relaxation is defined in the region between IVR₁ and IVR₂. Five frames (open circles) define four time steps (Δt_1 – Δt_4) spanning LVP during IVR for each beat.

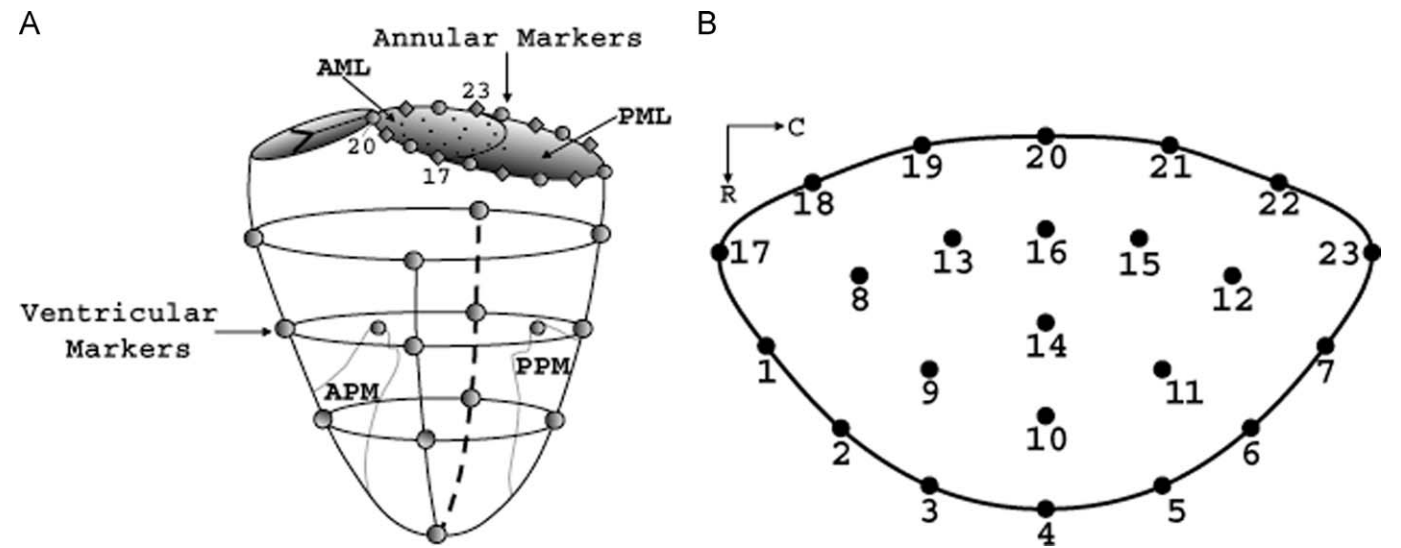


Fig. 1. Marker schematic. (A) Schematic showing ventricular and annular marker locations. Marker 20 is the anterior leaflet saddlehorn marker; markers 17 and 23 are the anterior and posterior commissural marker, respectively. AML = anterior mitral leaflet. PML = posterior mitral leaflet. (B) Schematic showing anterior leaflet marker grid and circumferential (C) and radial (R) axes.

defined as the earliest increase (above the systolic variation) in the separation between the central anterior and posterior leaflet edge markers.

To study the piecewise stress–strain behavior of the anterior mitral leaflet during IVR, for each beat, five frames were selected to span the IVR pressure range, defining four approximately 15 mmHg LVP increments associated with four successive time-intervals (Δt_1 – Δt_4) from IVR_2 to IVR_1 (Fig. 2). For the 24 beats analyzed, for time-step Δt_1 the group mean (\pm SD) transmitral pressure gradient (LVP–LAP) ranged from 0 (IVR_2) to 14 ± 1 mmHg; for time-step Δt_2 from 14 ± 1 to 30 ± 5 mmHg; for time-step Δt_3 from 30 ± 5 to 49 ± 6 mmHg; and for time-step Δt_4 from 49 ± 6 to 63 ± 6 mmHg.

2.4. Inverse finite element analysis

The inverse finite element analysis methodology to determine the material properties of the anterior mitral valve leaflet has been described in a previous publication (Krishnamurthy et al., 2008), thus will only be outlined here.

2.4.1. Finite element model

A finite element model of the anterior MV leaflet was developed for each individual time-step (Δt_1 , Δt_2 , Δt_3 , Δt_4) and for each beat using Hypermesh version 8.0 SR 1 (Altair Hyperworks; Troy, Michigan) to construct the geometry and meshing of the leaflet and Optistruct version 8.0 SR 1 (Altair; Troy, Michigan) as the solver. Thus, 96 individual finite element models (8 hearts, 3 beats/heart, 4 time-steps/beat) were analyzed for this study.

For each beat, the geometry of the anterior leaflet was initially defined by the leaflet marker positions (Fig. 1) at IVR_2 (assumed as the minimum–stress reference state). The x , y , z coordinate values for each of the leaflet and annular marker positions at IVR_2 were entered as points in Hypermesh. Five cubic splines were generated through (see Fig. 1B): (a) Markers 17–1–2–3–4–5–6–7–23; (b) Markers 18–8–9–10–11–12–22; (c) Markers 19–13–14–15–21; (d) Markers 19–16–21; and (e) Markers 19–20–21. These splines were used to generate a bicubic leaflet surface.

For the purpose of defining the MV leaflet material properties for Δt_1 , a coordinate system was defined with origin at the center of the 16 markers defining the saddle-shaped annulus (Levine et al., 1989) at IVR_2 . A line from the origin to marker #20 (the “saddlehorn”) was defined as the leaflet radial axis (R ; Fig. 1). The

leaflet circumferential axis (C ; Fig. 1) was defined normal to R and in the plane containing R and the posterior commissural marker (#23; Fig. 1).

A homogeneous leaflet was assumed, with an orthotropic linear elastic material model (MAT8 in Hypermesh). The bicubic surface fit of the MV leaflet was then meshed with plane-stress quadrilateral shell elements. A typical anterior leaflet was meshed with 2200 elements yielding an element size of 0.004 cm^2 .

The strut chordae were defined as structures undergoing pure tension (MAT1 in Hypermesh). A previously published *ex vivo* modulus (elastic modulus = 20 N/mm^2 ; cross-sectional area = 0.008 cm^2 (Kunzelman and Cochran, 1992)) was used for the strut chordae. Tension-only bar elements (PBARL in Hypermesh) were defined as radiating from the papillary muscle tip marker points (APM and PPM; Fig. 1A) to leaflet belly insertion positions (Fig. 3) defined from anatomical photographs.

The boundary conditions were then enforced on the finite element model. The measured transmitral pressure gradient (LVP–LAP) for the first time-step (Δt_1) was applied to the anterior mitral leaflet. The displacements of the annular markers (#17–23; Fig. 1B), anterior leaflet edge markers (#1–7; Fig. 1B) and papillary tip markers (APM and PPM; Fig. 1A) were defined using actual marker data at the end of Δt_1 .

The Hypermesh finite element model (Fig. 3) was then solved for the enforced boundary conditions using Optistruct to obtain the simulated displacements of the leaflet belly markers (#8–16; Fig. 1B). This initial run assumed nominal anterior leaflet material properties obtained from previous *ex vivo* studies (Kunzelman and Cochran, 1992).

2.4.2. Inverse finite element analysis algorithm

The Optistruct solver was then interlinked with commercial optimization software, Hyperstudy version 8.0 SR 1 (Altair Hyperworks, Troy, Michigan) to run an inverse finite element analysis to yield the *in vivo* material properties of the mitral valve during Δt_1 . In this algorithm, the model-simulated displacements of the nine leaflet belly markers (#8–16; Fig. 1B) from the nominal run were compared with the actual measured displacements of these 9 markers during time-step Δt_1 , to yield a response function defined as the root mean squared (RMS) displacement difference between measured and simulated displacements of the nine leaflet belly markers. Hyperstudy then used a parameter identification algorithm, the “Method of Feasible Directions” (Belegundu et al., 2004), to minimize the response function by repeated iterations of the material properties

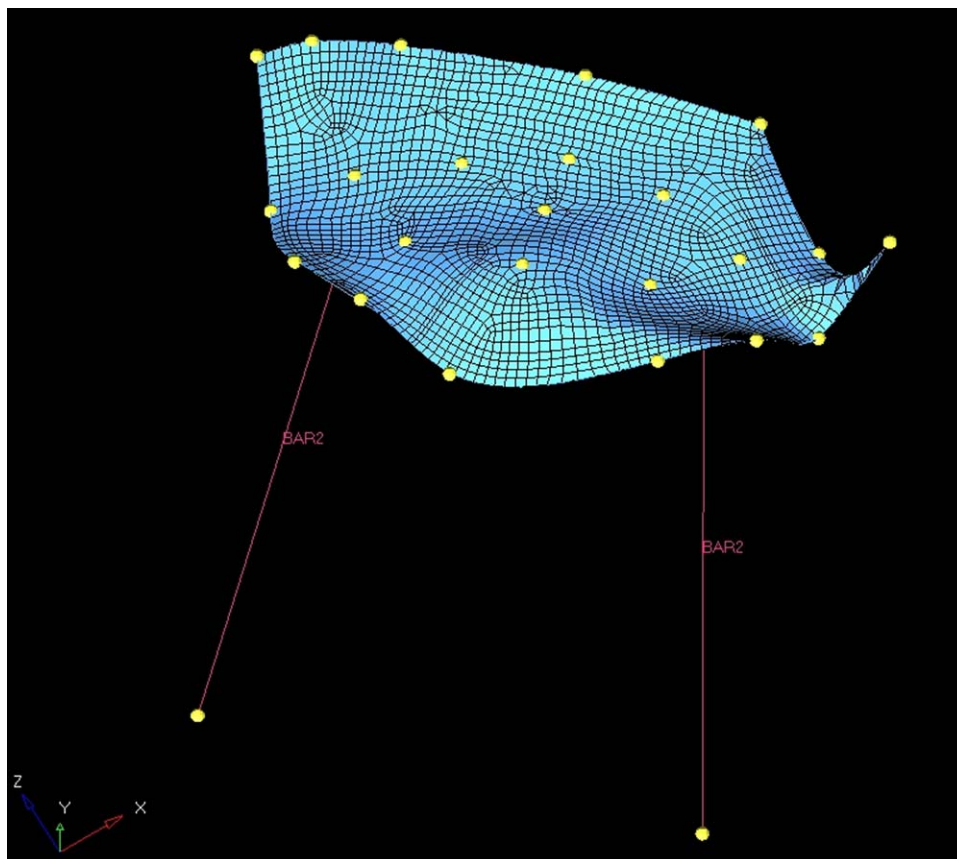


Fig. 3. FEA model. Typical finite element model of the anterior mitral valve leaflet. The meshed leaflet surface is depicted in blue. Red lines depict the strut chordae modeled as bar elements. Yellow dots indicate actual marker positions. (For interpretation of the references for colour in this figure legend the reader is referred to the web version of this article).

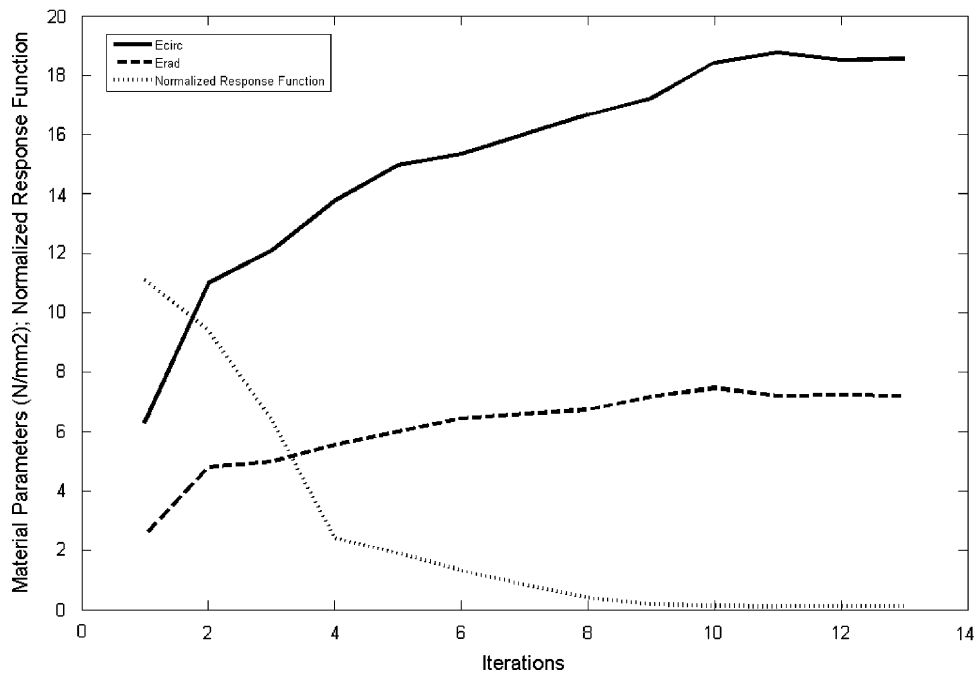


Fig. 4. Material parameter identification. Material properties (E_{circ} , solid line; E_{rad} , dashed line, N/mm²) and normalized response function (dotted line) versus number of iterations during a typical material parameter identification process.

(E_{circ} , E_{rad}) in the finite element model until a global minimum was obtained (Fig. 4). Leaflet circumferential-radial shear during IVR proved sufficiently small that E_{circ} and E_{rad} values so obtained were unchanged with inclusion or exclusion of this shear in the parameter identification process. The material property values (E_{circ} , E_{rad}) obtained at the end of the material identification run with the response function at its global minimum were interpreted as the *in vivo* material properties of the anterior MV leaflet belly during Δt_1 . That is, these material property values, when used in the finite element model for the anterior leaflet belly under the enforced pressure and geometric boundary conditions, produced, as closely as possible, the same displacements of the nine leaflet belly markers as those measured experimentally during time-step Δt_1 .

2.4.3. Forward analysis and stress–strain curve

The computed *in vivo* material properties were then used in the finite element model, to determine the stress and strain in the circumferential and radial directions for Δt_1 at marker #14 (as a representative case).

Using marker coordinates at the end of the previous time-step to build the finite element model for the next time-step, a similar inverse finite element analysis was employed to determine the material properties for each time-step during IVR, and forward analysis to determine the stresses and strains were performed for time-steps Δt_2 , Δt_3 and Δt_4 . The circumferential and radial stresses at marker #14 were plotted against the corresponding circumferential and radial strains at marker #14 for successive time-steps to construct piecewise circumferential and radial stress–strain curves for each beat.

The linearity of the stress–strain curve for each beat was characterized by the correlation coefficient (r^2) associated with a linear regression analysis of each curve.

3. Results

Table 1 displays the group mean heart rate, $-dP/dt_{max}$ during IVR, and left ventricular and left atrial pressures for each heart at IVR₁ and IVR₂. Variations in these parameters are seen from heart-to-heart, showing that the stress–strain curves represent a variety of hemodynamic conditions.

Table 2 gives the values of the circumferential and radial stresses and strains for the four transmitral pressure intervals associated with each of the 3 beats for the 8 hearts studied along with the r^2 correlation coefficient values for each curve. Fig. 5 displays these data as stress–strain plots, with each panel displaying the circumferential and radial stress–strain relations for each of the three beats from each heart. The group mean

(\pm SD) stress–strain linear correlation coefficient (r^2) values were 0.995 ± 0.003 for the circumferential curves and 0.994 ± 0.003 for the radial curves. The beat-to-beat reproducibility of the stress–strain curves in each heart (Fig. 5) validates the robustness of this method to study the stress–strain behavior of the anterior mitral leaflet during IVR. Consistent with results from *ex vivo* testing (May-Newman and Yin, 1995), *in vivo* radial strains are higher than circumferential strains at all time-steps.

4. Discussion

This study introduces a novel methodology using a combination of inverse and forward finite element analysis for the piecewise construction of stress–strain curves of the mitral valve leaflets, *in vivo*. Sacks and Enomoto (2006) reported, for the first time, the *in vivo* anterior leaflet strains, but the relationship between *in vivo* leaflet stresses and *in vivo* leaflet strains has not been reported so far. This is the first report of the stress–strain behavior of the anterior mitral valve leaflet in the beating heart. The key finding of the current study is that both circumferential and radial stress–strain curves are linear over a physiologic range of pressures, in the closed mitral valve. This finding validates the material linearity assumption made in our earlier study (Krishnamurthy et al., 2008) that determined the *in vivo* material properties of the anterior mitral leaflet during IVR.

The question may arise that because we made use of a linear elastic material model to quantify the material parameters, the overall stress–strain curves during IVR had to be linear. This is not the case. Each time-step analysis was independent. Thus, while each time-step yields a modulus based on a linear material model for that time-step, the next time-step could yield a completely different modulus. Thus, there is no requirement for the combined time-steps to exhibit linear behavior. If the relationship was truly non-linear, this approach used here should have detected this nonlinearity. Of interest, a prior study (Sacks et al., 2006) also demonstrated linear material behavior of the ovine anterior mitral

Table 1
Hemodynamics.

Study	Heart rate (min ⁻¹)	-dLVP/dt _{max} (mmHg/s) (IVR)	LVP _{IVR1} (mmHg)	LVP _{IVR2} (mmHg)	LAP _{IVR1} (mmHg)	LAP _{IVR2} (mmHg)
1.	77	1592 ± 46	82 ± 1	11 ± 0	10 ± 0	7 ± 1
2.	89	1560 ± 109	92 ± 1	11 ± 1	8 ± 0	8 ± 0
3.	107	1967 ± 123	67 ± 1	10 ± 1	2 ± 0	2 ± 1
4.	93	1103 ± 39	88 ± 1	12 ± 0	14 ± 0	9 ± 0
5.	95	1284 ± 53	87 ± 1	14 ± 1	11 ± 0	12 ± 0
6.	70	991 ± 19	84 ± 1	6 ± 1	8 ± 1	4 ± 1
7.	80	1621 ± 69	84 ± 2	4 ± 1	5 ± 1	4 ± 1
8.	82	1346 ± 327	95 ± 4	7 ± 1	8 ± 0	7 ± 0
Group mean ± S.D	87 ± 12	1433 ± 315	85 ± 8	9 ± 3	8 ± 3	7 ± 3

Heart rate, negative dLVP/dt_{max} (during IVR) and left ventricular and left atrial pressures at IVR₁ and IVR₂ for the three sequential beats analyzed from each heart.

Table 2
Raw stress and strain values.

Study	Beat	Time-step	Transmitral pressure (mmHg)	Circ. stress (kPa)	Circ. strain	r ² for circ. curves	Radial stress (kPa)	Radial strain	r ² for radial curves
1.	1	Δt ₁	0 → 12	118	0.008	0.983	121	0.015	0.993
		Δt ₂	12 → 20	310	0.015		300	0.034	
		Δt ₃	20 → 49	706	0.038		691	0.063	
		Δt ₄	49 → 60	1043	0.047		963	0.088	
	2	Δt ₁	0 → 12	102	0.004	0.991	114	0.016	0.997
		Δt ₂	12 → 20	279	0.01		279	0.034	
		Δt ₃	20 → 49	636	0.031		612	0.067	
		Δt ₄	49 → 59	943	0.042		911	0.096	
	3	Δt ₁	0 → 12	136	0.004	0.992	118	0.016	0.988
		Δt ₂	12 → 20	343	0.011		316	0.040	
		Δt ₃	20 → 49	757	0.033		717	0.070	
		Δt ₄	49 → 60	1059	0.044		1006	0.094	
2.	1	Δt ₁	0 → 14	124	0.004	0.996	117	0.016	0.998
		Δt ₂	14 → 32	407	0.011		408	0.057	
		Δt ₃	32 → 56	893	0.03		877	0.115	
		Δt ₄	56 → 73	1276	0.042		1172	0.147	
	2	Δt ₁	0 → 15	223	0.006	0.997	236	0.033	0.998
		Δt ₂	15 → 38	635	0.023		637	0.077	
		Δt ₃	38 → 67	1207	0.042		1195	0.139	
		Δt ₄	67 → 78	1529	0.049		1534	0.172	
	3	Δt ₁	0 → 14	196	0.006	0.993	192	0.032	0.997
		Δt ₂	14 → 32	473	0.017		468	0.066	
		Δt ₃	32 → 56	1039	0.04		1015	0.134	
		Δt ₄	56 → 73	1347	0.049		1292	0.165	
3.	1	Δt ₁	0 → 14	208	0.011	0.995	198	0.022	0.993
		Δt ₂	14 → 37	455	0.025		450	0.050	
		Δt ₃	37 → 54	738	0.037		718	0.072	
		Δt ₄	54 → 63	846	0.041		817	0.079	
	2	Δt ₁	0 → 15	187	0.008	0.997	179	0.022	0.991
		Δt ₂	15 → 28	406	0.019		384	0.043	
		Δt ₃	28 → 47	634	0.031		606	0.061	
		Δt ₄	47 → 58	871	0.04		818	0.078	
	3	Δt ₁	0 → 14	201	0.008	0.999	195	0.019	0.998
		Δt ₂	14 → 26	428	0.017		414	0.041	
		Δt ₃	26 → 40	682	0.026		660	0.066	
		Δt ₄	40 → 56	970	0.037		931	0.088	
4.	1	Δt ₁	0 → 12	132	0.007	0.999	128	0.025	0.992
		Δt ₂	12 → 26	318	0.016		297	0.049	
		Δt ₃	26 → 42	519	0.027		490	0.073	
		Δt ₄	42 → 55	774	0.04		736	0.103	
	2	Δt ₁	0 → 11	127	0.007	0.995	138	0.023	0.991
		Δt ₂	11 → 23	312	0.018		330	0.055	
		Δt ₃	23 → 39	531	0.027		561	0.088	
		Δt ₄	39 → 57	792	0.039		830	0.117	
	3	Δt ₁	0 → 12	149	0.008	0.992	156	0.022	0.998
		Δt ₂	12 → 27	320	0.017		334	0.044	
		Δt ₃	27 → 43	526	0.026		560	0.072	
		Δt ₄	43 → 56	748	0.034		797	0.098	
5.	1	Δt ₁	0 → 14	211	0.009	0.997	221	0.025	0.996
		Δt ₂	14 → 33	424	0.02		428	0.049	
		Δt ₃	33 → 46	653	0.031		661	0.07	
		Δt ₄	46 → 57	772	0.035		788	0.082	

Table 2 (continued)

Study	Beat	Time-step	Transmitral pressure (mmHg)	Circ. stress (kPa)	Circ. strain	r^2 for circ. curves	Radial stress (kPa)	Radial strain	r^2 for radial curves	
6.	2	Δt_1	0→12	108	0.005	0.997	99	0.014	0.991	
		Δt_2	12→29	305	0.014		302	0.043		
		Δt_3	29→44	528	0.025		533	0.069		
		Δt_4	44→59	750	0.038		744	0.088		
	3	Δt_1	0→14	201	0.012	0.998	209	0.029	0.994	
		Δt_2	14→33	399	0.021		398	0.052		
		Δt_3	33→46	632	0.033		639	0.076		
		Δt_4	46→57	738	0.038		750	0.087		
	7.	1	Δt_1	0→17	448	0.008	0.997	468	0.033	0.994
			Δt_2	17→31	843	0.015		871	0.058	
			Δt_3	31→49	1466	0.026		1478	0.095	
			Δt_4	49→68	2302	0.038		2311	0.136	
2		Δt_1	0→15	357	0.006	0.997	329	0.024	0.992	
		Δt_2	15→37	996	0.018		967	0.061		
		Δt_3	37→56	1544	0.027		1500	0.089		
		Δt_4	56→71	2056	0.034		2019	0.11		
3		Δt_1	0→15	372	0.007	0.997	392	0.024	0.995	
		Δt_2	15→36	1008	0.018		1044	0.062		
		Δt_3	36→54	1515	0.027		1543	0.091		
		Δt_4	54→69	2098	0.035		2135	0.116		
8.	1	Δt_1	0→14	427	0.01	0.997	403	0.044	0.993	
		Δt_2	14→30	986	0.022		944	0.093		
		Δt_3	30→45	1689	0.036		1643	0.146		
		Δt_4	45→58	2485	0.05		2430	0.203		
	2	Δt_1	0→15	492	0.011	0.998	472	0.047	0.997	
		Δt_2	15→32	1057	0.024		1061	0.096		
		Δt_3	32→47	1728	0.039		1722	0.151		
		Δt_4	47→61	2457	0.053		2461	0.204		
	3	Δt_1	0→15	468	0.011	0.996	445	0.055	0.993	
		Δt_2	15→33	1090	0.025		1050	0.115		
		Δt_3	33→48	1789	0.04		1753	0.178		
		Δt_4	48→62	2636	0.055		2574	0.243		
9.	1	Δt_1	0→13	512	0.009	0.996	488	0.037	0.996	
		Δt_2	13→32	1415	0.025		1400	0.113		
		Δt_3	32→49	2163	0.037		2133	0.165		
		Δt_4	49→64	2985	0.048		2934	0.215		
	2	Δt_1	0→13	454	0.008	0.997	433	0.039	0.994	
		Δt_2	13→33	1299	0.023		1234	0.1		
		Δt_3	33→51	2091	0.036		1942	0.147		
		Δt_4	51→67	2827	0.046		2651	0.19		
	3	Δt_1	0→14	488	0.008	0.999	455	0.038	0.994	
		Δt_2	14→33	1321	0.022		1261	0.105		
		Δt_3	33→51	2110	0.035		2062	0.162		
		Δt_4	51→66	2659	0.044		2696	0.197		

Stress and strain values for each time-step for 3 beats, 8 hearts, and 4 time intervals (Δt_1 – Δt_4). The transmitral pressure gradient, circumferential (Circ.) stress and strain, radial stress and strain and r^2 values for each stress–strain curve are shown.

leaflet in the closed valve, although their results are not directly comparable with the results of the present study as they plotted areal strain against LV pressure.

Next, we should comment on our choice of a minimum-stress, zero-strain reference state at IVR_2 (Fig. 2). First, to the best of our knowledge, it is impossible, using any technique currently available, to measure the loading on each side of the leaflet in the open valve. Moreover, leaflet shape in the open valve varies dramatically as it responds to complex blood flow patterns. Thus, we cannot perform a stress–strain analysis of the leaflet during diastole and thereby cannot establish whether a truly stress-free state exists at any time in an open valve. Thus, the current inverse finite element analysis methodology is applicable only to the closed mitral valve, when trans-leaflet pressures can be defined, and cannot be applied to the open mitral valve when trans-leaflet pressures are undefined and large geometric non-linearities may be present as observed in *in vitro* studies (He et al., 2003; Sacks et al., 2002). Second, to determine leaflet material properties using inverse FEA, we need to measure trans-leaflet pressures (both left

atrial and left ventricular) over the widest possible range. At IVR_2 , left atrial and left ventricular pressures are virtually equal (Fig. 2), yet the valve is still closed, thus the conditions at IVR_2 provide the nearest possible approximation to an unloaded state. Further, the interval between IVR_1 and IVR_2 provides the full physiological range of pressures encountered by the closed valve, allowing material properties to be estimated over this wide pressure range. Finally, it is possible, but difficult to imagine, that these thin membranous leaflets, have significant residual stress, relative to the stresses encountered when they are supporting LV pressures, although this possibility remains to be determined. For these reasons, then, we think that the choice of IVR_2 is appropriate as a minimum-stress minimum-strain reference configuration in FEA studies of mitral valve leaflet dynamics.

It must be noted that the leaflet edge has inconsistent deformations and mechanics. Taking this into account, we have reported stresses and strains only for the leaflet belly (marker 14; Fig. 1), as the belly region of the leaflet is homogeneous and has consistent deformations. In the FEA model, we incorporate the

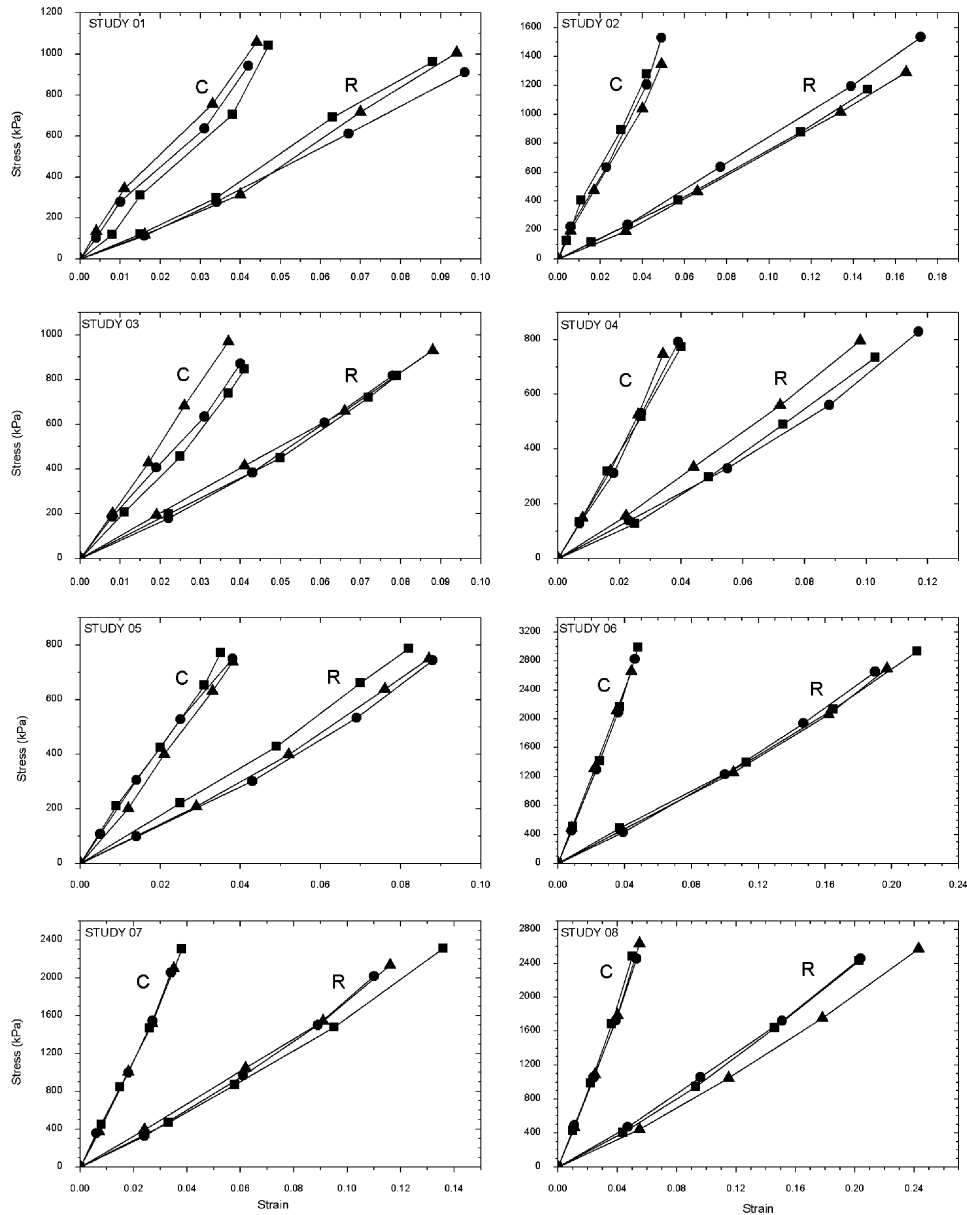


Fig. 5. Stress–strain curves. Stress vs. strain in the radial (R) and circumferential (C) directions. Data in each panel from three beats in specific heart.

actual motion of the leaflet edge as seen in our experiments to enforce accurate boundary conditions to the model, but understanding that the edge behavior is inconsistent we report only the stresses and strains at the center of the leaflet.

Finally, it has to be noted that leaflets are known to be heterogeneous with different regions of the leaflet having different material properties. Strut chordal insertions into the leaflet introduce material heterogeneities in the leaflet (Chen et al., 2004a,b). Scanning acoustic microscopy indicates that human anterior leaflets are stiffer in the fibrous middle layer than atrial and ventricular layers and the entire leaflet is stiffer at the annulus than at the free edge (Jensen et al., 2006). Leaflet homogeneity was a simplification for this initial effort to quantify the *in vivo* material behavior of the anterior mitral valve leaflet. Developing a heterogeneous finite element model is an ongoing effort in our group.

Conflicts of interest statement

None of the authors have any conflicts of interest.

Acknowledgments

The authors gratefully acknowledge the expert technical assistance of Sigurd Hartnett, BS, Maggie Brophy, AS, Eleazar Briones, BA, Lauren Davis, BS, and George T. Daughters, MS.

This study was supported by the National Heart, Lung and Blood Institute Grants HL-29589 and HL-67025. Gaurav Krishnamurthy was supported by the BioX Medtronic Graduate Fellowship, Wolfgang Bothe was supported by the Deutsche Herzstiftung, Frankfurt, Germany, and Julia C. Swanson was supported by the Western States Affiliate AHA Postdoctoral Fellowship.

References

- Belegundu, A.D., Damle, A., Rajan, S.D., Dattaguru, B., St Ville, J., 2004. Parallel line search in method of feasible directions. *Optim. Eng.* 5 (3), 379–388.
- Chen, L., McCulloch, A.D., May-Newman, K., 2004a. Nonhomogeneous deformation in the anterior leaflet of the mitral valve. *Ann. Biomed. Eng.* 32 (12), 1599–1606.
- Chen, L., Yin, F.C., May-Newman, K., 2004b. The structure and mechanical properties of the mitral valve leaflet-strut chordae transition zone. *J. Biomech. Eng.* 126 (2), 244–251.
- Daughters, G.T., Sanders, W.J., Miller, D.C., Schwarzkopf, A., Mead, C.W., Ingels, N.B.J., 1989. A comparison of two analytical systems for 3-D reconstruction from biplane videoradiograms. *IEEE Comput. Cardiol.* 15, 79–82.
- He, Z., Ritchie, J., Grashow, J.S., Sacks, M.S., Yoganathan, A.P., 2005. *In vitro* dynamic strain behavior of the mitral valve posterior leaflet. *J. Biomech. Eng.* 127 (3), 504–511.
- He, Z., Sacks, M.S., Baijens, L., Wanant, S., Shah, P., Yoganathan, A.P., 2003. Effects of papillary muscle position on *in-vitro* dynamic strain on the porcine mitral valve. *J. Heart Valve Dis.* 12 (4), 488–494.
- Jensen, A.S., Baandrup, U., Hasenkam, J.M., Kundu, T., Jorgensen, C.S., 2006. Distribution of the microelastic properties within the human anterior mitral leaflet. *Ultrasound Med. Biol.* 32 (12), 1943–1948.
- Krishnamurthy, G., Ennis, D.B., Itoh, A., Bothe, W., Swanson, J.C., Karlsson, M., Kuhl, E., Miller, D.C., Ingels Jr., N.B., 2008. Material properties of the ovine mitral valve anterior leaflet *in vivo* from inverse finite element analysis. *Am. J. Physiol. Heart Circ. Physiol.* 295 (3), H1141–H1149.
- Kunzelman, K.S., Cochran, R.P., 1992. Stress/strain characteristics of porcine mitral valve tissue: parallel versus perpendicular collagen orientation. *J. Card. Surg.* 7 (1), 71–78.
- Kunzelman, K.S., Einstein, D.R., Cochran, R.P., 2007. Fluid-structure interaction models of the mitral valve: function in normal and pathological states. *Philos. Trans. R Soc. London B Biol. Sci.* 362 (1484), 1393–1406.
- Levine, R.A., Handschumacher, M.D., Sanfilippo, A.J., Hagege, A.A., Harrigan, P., Marshall, J.E., Weyman, A.E., 1989. Three-dimensional echocardiographic reconstruction of the mitral valve, with implications for the diagnosis of mitral valve prolapse. *Circulation* 80 (3), 589–598.
- May-Newman, K., Yin, F.C., 1995. Biaxial mechanical behavior of excised porcine mitral valve leaflets. *Am. J. Physiol.* 269 (4 Pt 2), H1319–H1327.
- May-Newman, K., Yin, F.C., 1998. A constitutive law for mitral valve tissue. *J. Biomech. Eng.* 120 (1), 38–47.
- Niczyporuk, M.A., Miller, D.C., 1991. Automatic tracking and digitization of multiple radiopaque myocardial markers. *Comput. Biomed. Res.* 24 (2), 129–142.
- Prot, V., Skallerud, B., Holzapfel, G., 2007. Transversely isotropic membrane shells with application to mitral valve mechanics. Constitutive modelling and finite element implementation. *Int. J. Numer. Methods Eng.* 71, 987–1008.
- Sacks, M.S., Enomoto, Y., Graybill, J.R., Merryman, W.D., Zeeshan, A., Yoganathan, A.P., Levy, R.J., Gorman, R.C., Gorman III, J.H., 2006. *In-vivo* dynamic deformation of the mitral valve anterior leaflet. *Ann. Thorac. Surg.* 82 (4), 1369–1377.
- Sacks, M.S., He, Z., Baijens, L., Wanant, S., Shah, P., Sugimoto, H., Yoganathan, A.P., 2002. Surface strains in the anterior leaflet of the functioning mitral valve. *Ann. Biomed. Eng.* 30 (10), 1281–1290.
- Votta, E., Caiani, E., Veronesi, F., Soncini, M., Montevecchi, F.M., Redaelli, A., 2008. Mitral valve finite-element modelling from ultrasound data: a pilot study for a new approach to understand mitral function and clinical scenarios. *Philos. Transact. A Math. Phys. Eng. Sci.* 366 (1879), 3411–3434.